2021 43rd Annual International Conference of the
IEEE Engineering in Medicine & Biology Society (EMBC)
Oct 31 - Nov 4, 2021. Virtual Conference

Nuclei Segmentation on Histopathology Images of Breast Carcinoma*

V. Y. Ramirez Guatemala-Sanchez[1], H. Peregrina-Barreto[2] and G. Lopez-Armas[3]

Abstract— **With the use of computer-aided diagnostic systems, the automatic detection and segmentation of the cell nuclei have become essential in pathology due to cellular nuclei counting and nuclear pleomorphism analysis are critical for the classification and grading of breast cancer histopathology. This work describes a methodology for automatic detection and segmentation of cellular nuclei in breast cancer histopathology images obtained from the BreakHis database, the Standford tissue microarray database, and the Breast Cancer Cell Segmentation database. The proposed scheme is based on the characterization of Hematoxylin and Eosin (H&E) staining, size, and shape features. In addition, we use the information obtained from morphological transformations and adaptive intensity adjustments to detect and separate each cell nucleus detected in the image. The segmentation was carried out by testing the proposed methodology in a histological breast cancer database that provides the associated groundtruth segmentation. Subsequently, the Sørensen-Dice similarity coefficient was calculated to analyze the suitability of the results.**

Clinical relevance— **In this work, the detection and segmentation of cell nuclei in breast cancer histological images are carried out automatically. The method can identify cell nuclei regardless of variations in the level of staining and image magnification. Moreover, a granulometric analysis of the components allows identifying cell clumps and segment them into individual cell nuclei. Improved identification of cell nuclei under different image conditions was demonstrated to reach a sensitivity average of 0.76 ± 0.12. The results provide a base for further and complex processes such as cell counting, feature analysis, and nuclear pleomorphism, which are relevant tasks in the evaluation and diagnostic performed by the expert pathologist.**

I. INTRODUCTION

According to recent World Health Organization (WHO) data, breast cancer is the most common type of cancer in women [1], representing 15 % of all cancer cases. A correct breast cancer diagnosis is made by removing a small portion of the breast tissue through a standard procedure called a biopsy [2]. Once the tissue is obtained, it undergoes a process of conservation and staining to finally be observed under the microscope by the pathologist, who performs a visual evaluation of the tissue structures to classify and grade cellular differentiation [3] [4]. This evaluation is substantial to know the type of cancer and the degree of malignancy of breast carcinoma [5]. The pathologist performs a fundamental task for visual tissue analysis by evaluating the size and shape of the cellular nucleus. The recognition and evaluation of the tissue are done subjectively [6]. Hence, it is prone to possible diagnosis errors and discrepancies between experts. The diagnostic errors put the patient at risk of being subjected to incorrect or unnecessary treatments and interventions, a problem that has been recognized [7]. An oversaturation in health services generates an excessive workload for the medical expert, increasing the probability of human error [8]. The image analysis techniques and computer vision have been widely recognized in medical research since they provide an advantage in quantitative analysis and aid the final diagnosis of the experts [3]. Automatic detection of the cell nuclei is a critical tool to perform an automated analysis of breast tissue histological sections. So, cell nuclei analysis is a relevant task in the classification and grading of breast cancer.

Several approaches have been proposed for automatic nuclei detection and segmentation on H&E staining images by using computational techniques such as gradient-based methods [9], morphological operations [10], active contours [11], [12],among others. Other approaches use marker-controlled watershed to segment the nuclei [13], [14] varying the way to produce markers such as fast radial symmetry [15], [16] or template matching [17]. However, the techniques used by the methods have fixed parameters. Some of them require a prior manual or partial identification of the nuclei, which is a limitation when a new dataset is analyzed. Moreover, some methods identify the nuclei, but they do not consider separating clusters or clumps of particles which is a significant restriction.

In this work, we propose an automatic methodology to detect and segment cell nuclei in breast cancer histopathology images. Our goal is to provide a method capable of identifying the cellular structures of interest and segmenting them independently of parameters such as the magnification of the sample or the staining level. Moreover, the proposed method deals with identifying and dividing cell clusters, a common issue in histopathological samples.

II. BASIC CONCEPTS

A. Histopathology

Histopathology is the study of the signs of disease in tissue when analyzed under a microscope [24]. The biopsy obtained from the patient is processed and fixed on glass slides. It is necessary to distinguish the tissue components with different colorants intended to highlight the cellular structure. A handy H&E staining technique whose main characteristic is that

*This work was not supported by any organization

[1]V. Y. Ramirez Guatemala-Sanchez and [2]H. Peregrina-Barreto are with Computer Science Department, Instituto Nacional de Astrofísica Óptica y Electrónica, Luis Enrique Erro 1, Santa Maria Tonantzintla, 72840 Puebla, Mexico, yurasamai@gmail.com, hperegrina@ieee.mx

[3]G. Lopez-Armas Researcher is with Faculty of Engineering, Centro de Enseñanza Técnica Industrial, Nueva Escocia 1885, Guadalajara, Jal. glopez@ceti.mx

hematoxylin remarks cell nuclei in dark purple and blue tones while eosin stains the cytoplasm and connective tissue in pink tones (Fig. 1) [3]. Large amounts of data have been analyzed under this technique, and given its usefulness, it is expected to continue to be a gold standard in tissue analysis [25].

Fig. 1. H&E stained histology image of lobular carcinoma [35].

B. Mathematical morphology

The mathematical morphology is widely used in image analysis since it is useful to represent and describe the structures in the image. By using morphological operations, we can simplify images while preserving their main features. A morphological transformation involves the interaction between the structures (objects) in the image A and an analysis window called structuring element B that indicates the morphology (shape) used for processing A [26]. The shape of the structuring element may be circular, diamond, line, although a square shape is typically used [27]. Two basic morphological operations are called morphological opening (1) and morphological closing (2) where λ is a parameter associated to the scale of B . On (1) and (2), the transformations of erosion $\varepsilon_{\lambda B}$ and dilation $\delta_{\lambda B}$ are defined as $\varepsilon_{\lambda B}(f)(x) = min\{f(y); y \in \lambda B\}$ and $\delta_{\lambda B}(f)(x) = max\{f(y); y \in \lambda B\}$ where max and min take the maximum and minimum values, respectively . Dilation grows or enlarges an object by increasing its area, for example, to connect two or more objects, becoming them into one. Erosion reduces the object area, which is useful when two or more objects must be separated. For instance, some objects are connected when dilation is applied, but others only are enlarged. In some applications, it is important not to change the size of the objects significantly. Then, to avoid such an effect, the complementary transformation, i.e., erosion, is applied after dilation or vice versa. The restoration of the objects size is associated with the second operation in a morphological opening or closing.

$$\gamma_{\lambda B}(f) = \delta_{\lambda B}\left[\varepsilon_{\lambda B}(f)\right] \tag{1}$$

$$\varphi_{\lambda B}(f) = \varepsilon_{\lambda B}\left[\delta_{\lambda B}(f)\right] \tag{2}$$

C. Granulometry

Granulometry is a measure based on morphological operations and is used to know the grain sizes in the image. Grain is generally seen as a piece of solid or liquid matter, and size is understood as the characteristic dimension of the grain [28]. In the case of spherical particles, the radius will be taken as the dimension related to its size. In digital image processing, the meaning of grain changes to refer to a structure or object associated with a particular (solid) gray level. For instance, on a microscope image, a cell is represented by a certain gray level or staining. The granulometric analysis allows us to estimate the size of the objects in the image, which is important in subsequent processes such as segmentation, analysis of the distribution, or focusing a certain process towards a particular object size. Granulometry is defined as a set of operations $\{\gamma_\lambda\}$ with λ of some ordered set A. The granulometric analysis of an image f can be seen as a mapping of the morphological apertures in $\{\gamma_\lambda\}$ and a measurement mes of the area or volume of the image at opening $\gamma_\lambda(f)$. The difference between an opening of λ size ($mes(\gamma_\lambda(f))$ and an opening of incremental size $\lambda + \Delta$ ($mes(\gamma_{\lambda+\Delta}(f))$ indicates the impact of the changes in the image, associating the impact to the $\lambda + \Delta$ size. The obtained difference is called pattern spectrum ($PS(f)$) (3). To recognize the amount of structures of representative size λ that are present in the image, $PS(f)$ is normalized by ($mes(f)$).

$$PS(f) = \frac{mes(\gamma_\lambda(f)) - mes(\gamma_{\lambda+\Delta}(f))}{mes(f)} \tag{3}$$

D. Watershed

Watershed is a segmentation technique that identifies regions based on mathematical morphology; it allows establishing the boundaries among the regions on the image. Watershed classifies pixels according to their spatial proximity, the gradient of their gray levels, and the homogeneity of their texture [29]. Watershed considers that a grayscale image I can be seen as a topological surface where every local minimum (darker regions) is the bottom of a valley or a catchment basin (Fig. 2a). Then, starting with the minimum intensity value, each catchment basin is marked or flooded. This flood will progressively fill different catchment basins of the image (Fig. 2b-c). When the flood reaches the maximum level in a basin (higher gray level), a watershed must be marked to avoid flooding another vessel (Fig. 2d-e). In this way, the borders are found, and the objects are segmented (Fig. 2f) [31]. The watershed transformation is denoted by (4), where the watershed of f is the set of points that do not belong to any regional minimum catchment basin $CB(m_i)$. A regional minimum catchment basin is defined as the set of points in a connected domain D that is topologically closer to the regional minimal (m_i) than any other m_j [32].

$$Wshed(f) = D \cap \left(\bigcup_{i \in I} CB(m_i)\right)^c \tag{4}$$

III. Methodology

The proposed method consists of three principal parts: (A) a local intensity adjustment to highlight regions of interest followed by a granulometric analysis to know the particles size in the histological image. (B) A selective process to identify particles of interest and discard those that do not

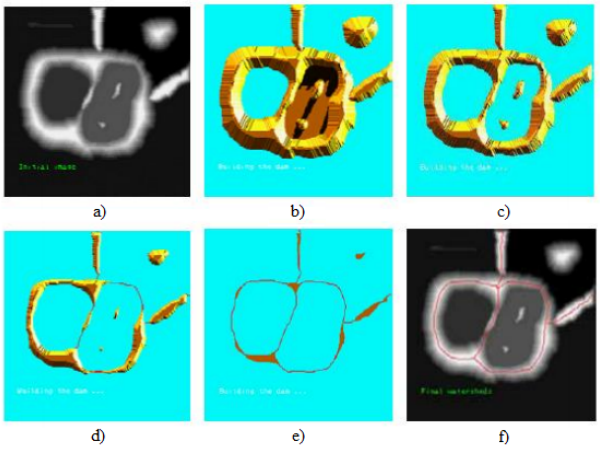

Fig. 2. Flooding process for object segmentation by the watershed transform [31]. **a)** Gray level intensity image **b-c)** flooding starts from the lowest minimum local, and every catchment basin is marked, **d-e)** flood reaches the maximum level of the catchment basin and stops flooding **f)** after every catchment basin is flooded, the remaining borders denote different regions, and segmentation is done.

provide relevant information; (C) a refinement of segmentation focused on dividing the larger objects associated with clumps or overlapped nuclei. Figure 3 shows the framework of the proposed methodology. Every stage is described in detail below.

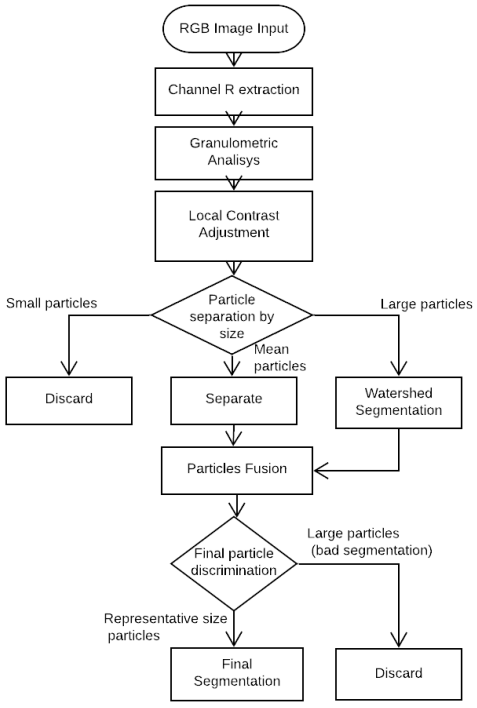

Fig. 3. Proposed automatic cell nuclei segmentation.

A. Separation by color

H&E staining system is characterized by highlighting the tissue components in purple tones, darker in the nucleus area, and pink in the cytoplasm and related tissue surrounding the nucleus. Therefore, the separation of the red channel of the color image helps to highlight the purple hue to easily extract the components of interest. Figure 4 shows an original histopathological RGB image (left) and its corresponding red channel (right). It is observed that in the red channel, there is a high contrast between the components of interest (cell nuclei in dark grays) and the rest of the elements (tissue and background in light grays). However, it is difficult to distinguish the limits among the components of interest in some areas, an issue that often affects the segmentation results.

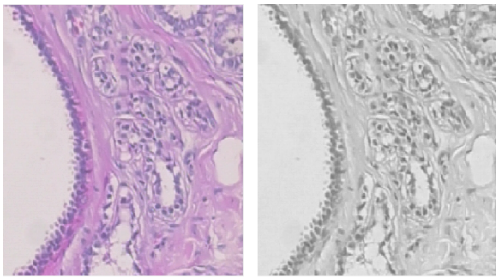

Fig. 4. Red channel separation from a color image. **a)** RGB Image, and **b)** channel R extraction.

B. Local contrast adjustment

Once the red channel has separated, it seeks to improve the contrast in the regions that correspond to the cell nucleus. Then, a contrast adjustment is applied by using a gamma correction function whose simplest form is defined by the power function $V_{out} = AV_{in}^{g}$; where V_{in} is a real positive value, A is a constant and g is the gamma encoding that symbolizes a numeric parameter [33]. The gamma correction highlights objects of interest by doing a linear mapping low to bottom and high to top of the values of its pixels. The gamma correction function $GC(I, r)$ performs a linear mapping (Gamma = 1) of the values in the image I to the range $r = [low_{in}, high_{in}]$ where $low_{in} = m - (std * 2)$ and $high_{in} = m$, m is the average of the intensity values of the image and std is the standard deviation. However, it must be taken into account that cells nuclei are surrounded by neighborhoods of pixels with different gray levels. Therefore, if a general adjustment is applied taking statistics from the whole image, cells nuclei on low contrast areas may become more similar to the background, making their subsequent segmentation difficult. A more accurate approach consists of dividing the image into subregions for a local contrast adjustment. In this way, it is possible to deal with the gray level differences within a smaller area and enhance the contrast among its components, i.e., cell nucleus and background. The subregion size is an important parameter because it is expected that several components of interest are contained on it, and this depends on the image magnification. Then, this is a dynamic parameter. A granulometric analysis is performed to estimate the size distribution of the particles in the image and ensure that the subregion size is larger than

any cell nucleus on the image. A circular structural element was used in this analysis since it was according to the cell nucleus morphology. Figures 5a-b shows the granulometric analysis of the original image where the most relevant size corresponds to a structural element of radius $r = 4$, meaning that most of the cell nuclei could be contained on an area of 7×7. After several tests, an optimal contrast adjustment was obtained by processing subregions covering an area of 25 times the cell nucleus size r. Thus, the subdivision of the image is independent of the magnification.

Once the image has been divided into subregions (Fig. 5c), the contrast adjustment is performed locally, increasing the gray level distance between the components according to their particular conditions. For example, in Fig. 5 the cell nuclei at the center of the histological section were low contrasted with respect to those at the edge. After local contrast adjustment (Fig. 5d), the cell nuclei in both areas were highlighted from their respective background, showing the advantage of using the local information for improvement. This result facilitates the binary segmentation of the image that extracts the components most likely related to a cell nuclei, eliminating the background and other tissue parts that are not of interest. (Fig. 5e).

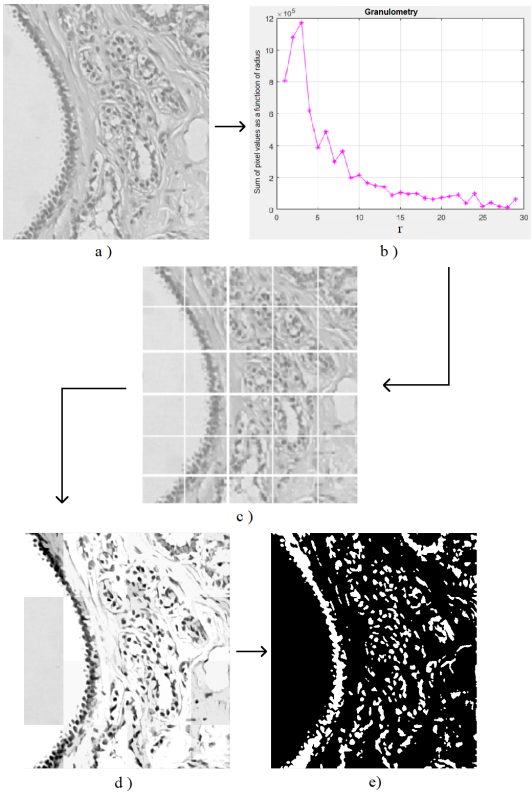

Fig. 5. Scheme of the process for local contrast adjustment. **a)** Initial R channel image, **b)** granulometry, **c)**sub-section separation using granulometry measure as reference, **d)**local adjustment result, **e)** image binarization.

C. Adaptive segmentation

where m_c is the mean circularity of all particles and s_c is the standard deviation. The cell nuclei that do not

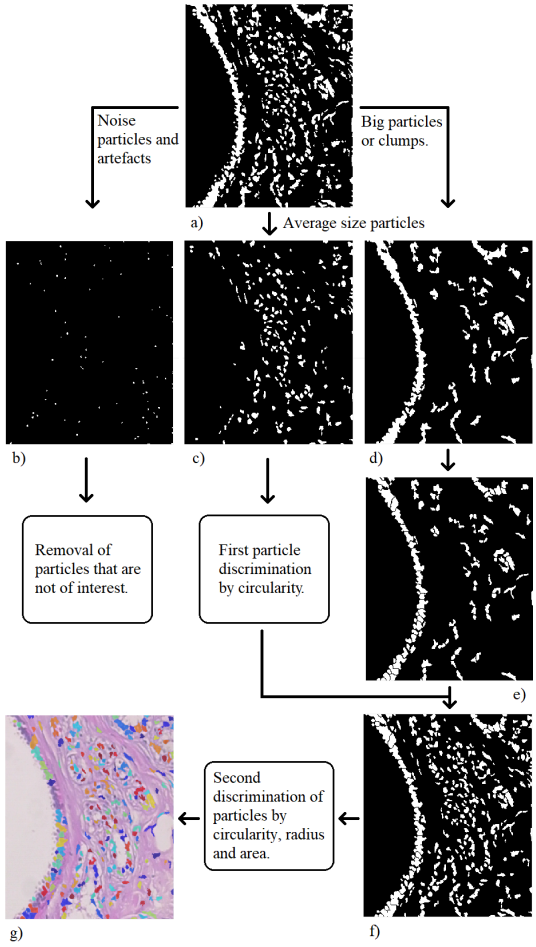

Fig. 6. Selection and Watershed segmentation, **a)** binary Image, **b)** small particles, noise and possible artefacts, **c)** average size particles are saved, **d)** big particles and clumps for separation with Watershed, **e)** segmented clumps, **f)** resulting particles of previous processes are fused, **g)** resulting segmentation.

fulfill the threshold are eliminated. The components of size larger than r could be associated with clusters of nuclei overlapped or very close to each other (Fig. 6d). If larger components are removed, important information may be lost. Then, it is important to identify the inner cell nuclei that these components may contain and divide them. Watershed segmentation is performed using the binary image as a marker over the red channel image to address this problem. As observed in Fig. 6e, most of the particles were divided by watershed. Nevertheless, it must be considered that not all divisions correspond to a cell nucleus; some could be part of tissue or background and must be removed. Since the particle size information may change due to the segmentation, a new granulometric analysis is performed over the fused image containing all the particles of interest (Fig. 6f) to ensure that the representative size of cell nuclei is known. The circularity threshold is recalculated over the segmented clumps to preserve only the rounder and larger cell nuclei (Fig. 6g). The area threshold is determined by calculating the mean and standard deviation of the areas of every detected

particle. In this way, we discard possible clumps that have not successfully segmented or some particles that may have been over-segmented.

IV. Tests and Results

The proposed methodology was tested on a subset of three different databases containing H&E stained microscopic images of histological sections of breast cancer. The BreakHis database [35] contains 9109 images with a resolution of 700x460 pixels, 24 bit depth and with about 82 different cases (patients); these images have different magnification at 40x, 100x, 200x, and 400x. The Standford tissue microarray database [36] contains 143 mammary carcinoma specimens with a resolution of 2256x1440 pixels and 24-bit depth, and the Breast Cancer Cell Segmentation database contains 58 images with a resolution of 896x768 pixels and 24-bit depth and their corresponding segmentation groundtruth [37]. A subset of 107 images was selected from the BreakHis databases, 29 images from the Standford tissue microarray database, and all specimens from the Breast Cancer Cell Segmentation database were used to assess the performance of the proposed method.

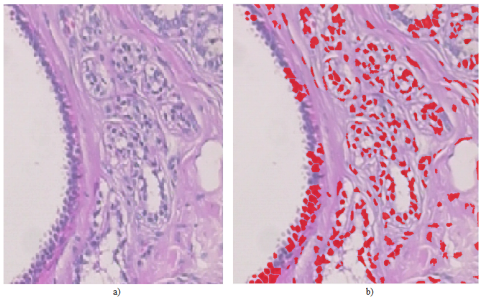

Fig. 7. Papillary carcinoma segmentation image from BreakHis Database [35]: **a)** Original image and **b)** the red markers of its cell nuclei obtained after segmentation.

With the aim of test the proposed method under different tissue conditions, there were analyzed images of papillary and malignant carcinoma as well as benign tumors (Figs. 7-9). As observed, there are differences in the images related to the size of cell nuclei, staining contrast, and magnification. Also, there are differences generated by the acquisition device, such as image resolution and bit depth-related to image quality. For example, in Fig. 7 the edge of the histological section (dark purple) presents low contrast, making difficult its segmentation in individual components in some areas. However, in the central area, the majority of the components of interest were segmented. Figure 8 shows higher contrast between the components, and the proposed method achieves the segmentation of almost all the cell nuclei. Furthermore, the granulometric analysis allows achieving relevant results even when the magnification changes. For example, in Fig. 9 is shown a histological section containing larger nuclei where most of them were segmented. Observing those cell nuclei that could not be segmented has particular characteristics such as elongated shapes that did not match a circular criterion or clusters where the contrast could not be improved even using a local contrast adjustment. One particular characteristic of this last case is that some nuclei have low staining and are surrounded or contain an even lighter area. Then, they are not identified as components of interest.

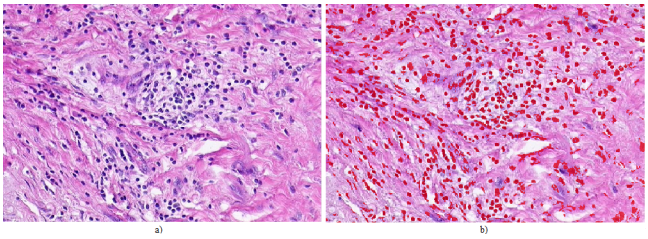

Fig. 8. Breast malignant carcinoma image from the Stanford Tissue Microarray Database [36]: **a)** Original image and **b)** its segmentation superposed.

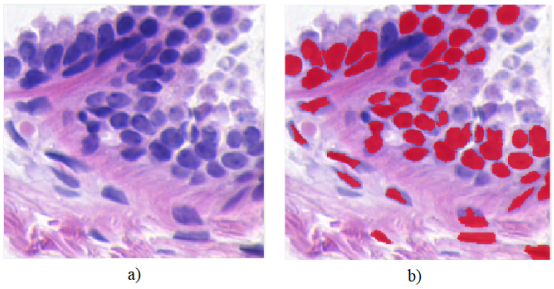

Fig. 9. Benign breast tumor image from Breast Cancer Cell Segmentation Database [37]: **a)** Original image and **b)** its segmentation superposed.

A. Results evaluation

Groundtruth images, which were provided by the database in [37], were used to evaluate the quality of the obtained segmentation. Let denote S_s as the segmentation obtained by the proposed method and S_t as the segmentation associated with the groundtruth. An area-based metric was used to analyze both segmentations by calculating the area of true positives (TP) as $S_{TP} = S_s \cap S_t$, false positives (FP) as $S_{FP} = S_s - S_t$, true negatives (TN) as $S_{TN} = S_t - S_s$, and false negatives (FN) as $S_{FN} = E - S_s - S_t$ where E denotes the region that includes all possible segmented regions. The precision, sensitivity and similarity Sørensen–Dice coefficient (SDC) (5-7), a measure of similarity between two sets in the range $[0, 1]$ [38], [39], are computed.

$$DSC = \frac{2 \cdot TP}{2 \cdot TP + FP + FN} \tag{5}$$

$$Precision = \frac{TP}{TP + FP} \tag{6}$$

$$Sensibility = \frac{TP}{TP + FN} \tag{7}$$

Figure 10 shows two examples of original images (left) and the image comparison between the obtained segmentation (center) and its corresponding groundtruth (right). It is observed a high similarity between results, although they differ in how some components are presented. For example,

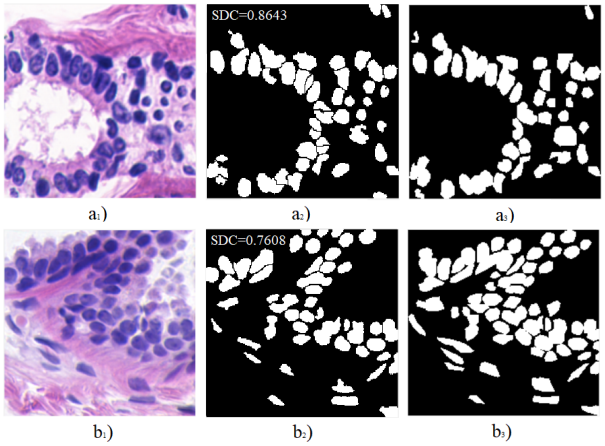

Fig. 10. a_1, b_1) Original histological images , a_2, b_2) the segmentation results by the proposed method , and a_3, b_3) their corresponding groundtruth.

the groundtruth contains larger components associated with nuclei clusters while the obtained segmentation divides most of them. As mentioned before, a circularity criterion is used since most of the components of interest have a high circular degree. Therefore, elongated nuclei are not contained in the obtained results. These differences are reflected in the value of the Sørensen-Dice coefficient. For the first example in Fig.10, it is observed a high similitude ($SDC = 0.8643$) with the groundtruth where the main difference is the division that watershed reaches in some clusters. The difference in the second example is higher, causing a lower $SDC = 0.7608$. Nevertheless, there is a notorious difference in the number of nuclei because of the circularity criterion that must be fulfilled and the cluster division reached by the proposed method. Then, these two processes are related to a lower SDC since they remove part of the pixels in the segmented image, but in return, accuracy is gained in the correct identification of the nuclei. The results were measured quantitatively through SDC values and compared with the obtained measures using Active Contours [40] with $SDC = 0.6$ and Otsu method [41] with $SDC = 0.7$. Table I shows the statistics about segmented cell nuclei of the whole database with and without considering the watershed segmentation that allows cluster division. There was not a significant difference between the SDC values, meaning that the cell nuclei cluster division does not affect the evaluation but could improve cell nuclei identification. An example of this is shown in the comparison of Fig. 11 where the proposed method reaches an accurate cell nuclei identification even in overlapping or closer particles. Therefore, eliminating nuclei that are not round enough contributes the most to the difference in SDC values. Nevertheless, this is not a negative contribution since eliminating non-round components avoids the inclusion of artifacts (e.g., incomplete cell nuclei), ensuring that only well-identified cell nuclei remain in the final segmentation. Moreover, after several tests, it was found that some cell nuclei are not present in the ground truth, and the proposed method was able to detect them (Fig. 12). This is another factor associated with the similarity measure decay because it increases the difference between the groundtruth and the resulting segmentation. However, the elimination of elongated components and improvement in the detection of nuclei are positive characteristics in terms of the contribution of the method.

TABLE I

COMPARISON OF THE NUCLEI SEGMENTATION WITH AND WITHOUT CLUSTER DIVISION AND WITH OTHER SEGMENTATION METHODS.

Measure	No Cluster Seg.	Cluster Seg.	Active Contours	Otsu Method
Sørensen-Dice Coefficient	0.78 ±0.07	0.75 ±0.08	0.611 ±0.2	0.7 ±0.1
Precision	0.73 ±0.09	0.75 ±0.09	0.5 ±0.2	0.56 ±0.1
Sensitivity	0.83 ±0.1	0.76 ±0.12	0.9 ±0.1	0.7 ±0.1

mean±standard deviation

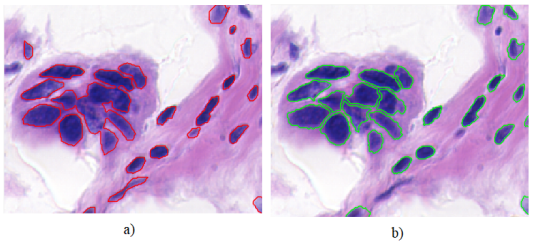

Fig. 11. Clump separation comparative. **a)** Ground truth and **b)** resulting segmentation with proposed method.

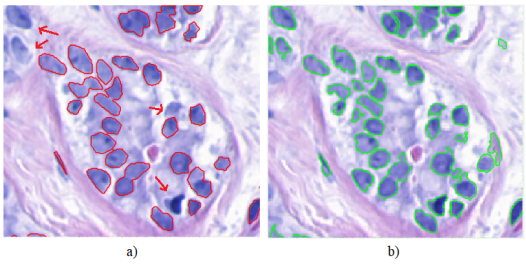

Fig. 12. Particle detection comparative. **a)** Ground truth and **b)** resulting segmentation with proposed method.

V. CONCLUSIONS

The high variation of intensity and characteristic forms of the mammary cell tissue represents a challenge for the automatic characterization and segmentation of the cell nuclei. Nonetheless, the general quality of the segmentation depends on the robustness of the method to handle this type of variation. The segmentation results achieved with the proposed method are consistent under different image conditions such as density of cells, magnification, and contrast, making it useful in pathological analysis. A suitable cell nuclei identification was reached by applying contrast adjustment and morphological analysis that is automatically adapted to the particular image conditions. Also, the comparison with

a groundtruth shows a high similitude of the results. Other similarity measures that may better reflect the significance of the differences found will be tested in future work.

ACKNOWLEDGMENT

V. Y. Ramirez Guatemala-Sanchez thanks the CONACYT for the scolarship 1008115.

REFERENCES

[1] Cancer de mama: prevención y control. Organización Mundial de la Salud. https://www.who.int/topics/cancer/breastcancer/es/

[2] "¿How is Breast Cancer Diagnosed?". Septembrer 14, 2020. Division of Cancer Prevention and Control, Centers for Disease Control and Prevention. https://www.cdc.gov/cancer/breast/basic_info/diagnosis.htm

[3] Gurcan, M. N., Boucheron, L. E., Can, A., et al.. Histopathological Image Analysis: A Review. IEEE Reviews in Biomedical Engineering, 2, 147–171 (2009).

[4] Veta, M. et al. "Breast Cancer Histopathology Image Analysis: A Review." IEEE Transactions on Biomedical Engineering 61 (2014): 1400-1411.

[5] Elston CW, Ellis IO. Pathological prognostic factors in breast cancer. I. The value of histological grade in breast cancer: experience from a large study with long-term follow-up. Histopathology. 1991;19(5):403-410.

[6] Slaoui, Mohamed & Fiette, Laurence (2011). Histopathology Procedures: From Tissue Sampling to Histopathological Evaluation. Methods in molecular biology (Clifton, N.J.). 691. 69-82. doi:10.1007/978-1-60761-849-24. (2011)

[7] Singh, H., Schiff, G. D., Graber, M. L., et al. The global burden of diagnostic errors in primary care. BMJ Quality & Safety, 26(6), 484–494 (2016).

[8] Chris Rohads. Overworked Doctors & Nurses Cause Serious Medical Mistakes. (2019). Available in: https://www.rhoadsandrhoads.com/blog/overworked-doctors-nurses-cause-serious-medical-mistakes

[9] Ali, S. and A. Madabhushi. "An Integrated Region-, Boundary-, Shape-Based Active Contour for Multiple Object Overlap Resolution in Histological Imagery." IEEE Transactions on Medical Imaging 31 (2012): 1448-1460.

[10] Irshad, H.. "Automated mitosis detection in histopathology using morphological and multi-channel statistics features." Journal of Pathology Informatics 4 (2013).

[11] Cosatto, E. et al. "Grading nuclear pleomorphism on histological micrographs." 2008 19th International Conference on Pattern Recognition (2008): 1-4.

[12] Qi, X. et al. "Robust Segmentation of Overlapping Cells in Histopathology Specimens Using Parallel Seed Detection and Repulsive Level Set." IEEE Transactions on Biomedical Engineering 59 (2012): 754-765.

[13] Yang, X. et al. "Nuclei Segmentation Using Marker-Controlled Watershed, Tracking Using Mean-Shift, and Kalman Filter in Time-Lapse Microscopy." IEEE Transactions on Circuits and Systems I: Regular Papers 53 (2006): 2405-2414.

[14] Huang, P. and Y. Lai. "Effective segmentation and classification for HCC biopsy images." Pattern Recognit. 43 (2010): 1550-1563.

[15] Veta, M. et al. "Marker-controlled watershed segmentation of nuclei in H&E stained breast cancer biopsy images." 2011 IEEE International Symposium on Biomedical Imaging: From Nano to Macro (2011): 618-621.

[16] Veta, M. et al. "Automatic Nuclei Segmentation in H&E Stained Breast Cancer Histopathology Images." PLoS ONE 8 (2013): n. pag.

[17] Kachouie, Nezamoddin N. et al. "Constrained watershed method to infer morphology of mammalian cells in microscopic images." Cytometry Part A 77A (2010): n. pag.

[18] Naik, S. et al. "Automated gland and nuclei segmentation for grading of prostate and breast cancer histopathology." 2008 5th IEEE International Symposium on Biomedical Imaging: From Nano to Macro (2008): 284-287.

[19] Wang, Pin et al. "Automatic cell nuclei segmentation and classification of breast cancer histopathology images." Signal Process. 122 (2016): 1-13.

[20] Kowal, M. and P. Filipczuk. "Nuclei segmentation for computer-aided diagnosis of breast cancer." Int. J. Appl. Math. Comput. Sci. (2014).

[21] Faridi, P. et al. "An automatic system for cell nuclei pleomorphism segmentation in histopathological images of breast cancer." 2016 IEEE Signal Processing in Medicine and Biology Symposium (SPMB) (2016): 1-5.

[22] Salvi, M. and F. Molinari. "Multi-tissue and multi-scale approach for nuclei segmentation in H&E stained images." BioMedical Engineering OnLine 17 (2018): n. pag.

[23] Kumar, N. et al. "A Dataset and a Technique for Generalized Nuclear Segmentation for Computational Pathology." IEEE Transactions on Medical Imaging 36 (2017): 1550-1560.

[24] Histopathology. The Royal College of Pathologists. https://www.rcpath.org/discover-pathology/news/fact-sheets/histopathology.html

[25] H. Fox, "Is H& E morphology coming to an end?," Brit. Med. J., vol.53, p. 38, (2000).

[26] R. Owens. Mathematical Morphology (1997). Avaliable at: http://homepages.inf.ed.ac.uk/rbf/CVonline/LOCAL%COPIES/OWENS/LECT3/node3.html

[27] R. Fisher, S. Perkins, A. Walker and E. Wolfart. Morphology (2003). Avaliable at: http://homepages.inf.ed.ac.uk/rbf/HIPR2/morops.htm

[28] P. Maragos, "Pattern spectrum and multiscale shape representation," IEEE Trans. Pattern Anal. Mach. Intell. 11, 701–716 (1989).

[29] N. La Serna, L. P. Concepción. "Watershed: an algorithm efficient and flexible segmentat8ion of footage gels 2-OF". (2010).

[30] Jiménez Hernández, Sofía. Aplicación de técnicas de procesado de imagen para las segmentación de núcleos en muestras histológicas humanas. Diss. (2016).

[31] Amandep, K. "Image Segmentation Using Watershed Transform." International Journal of Soft Computing and Engineering (IJSCE). University Putiala, India 4.1 (2014).

[32] Roerdink, J. and Arnold Meijster. "The Watershed Transform: Definitions, Algorithms and Parallelization Strategies." Fundam. Informaticae 41 (2000): 187-228.

[33] 2- Poynton, C.. "Digital Video and HDTV Algorithms and Interfaces." (2003).

[34] Olson, E.. "Particle Shape Factors and Their Use in Image Analysis – Part 1 : Theory." (2013).

[35] Spanhol, F., Oliveira, L. S., Petitjean, et al. A Dataset for Breast Cancer Histopathological Image Classification, IEEE Transactions on Biomedical Engineering (TBME), 63(7):1455-1462, (2016).

[36] Robert J. Marinelli, Kelli Montgomery, Chih Long Liu, et al. The Stanford Tissue Microarray Database. Nucleic Acids Res 2008 36(Database issue): D871-7. Epub (2007) Nov 7 doi:10.1093nargkm861

[37] Breast Cancer Cell Segmentation. Elisa Drelie Gelasca and Jiyun Byun and Boguslaw Obara and B.S. Manjunath. Avaliable at: http://bioimage.ucsb.edu/research/bio-segmentation

[38] Sørensen, T. . "A method of establishing groups of equal amplitude in plant sociology based on similarity of species and its application to analyses of the vegetation on Danish commons". Kongelige Danske Videnskabernes Selskab. (1948).

[39] Dice, Lee R. Measures of the Amount of Ecologic Association Between Species. Ecology. 26 (3): 297–302. doi:10.2307/1932409. JSTOR 1932409. (1945).

[40] Kass, M. et al. "Snakes: Active contour models." International Journal of Computer Vision 1 (2004): 321-331.

[41] Otsu, N.. "A threshold selection method from gray level histograms." IEEE Transactions on Systems, Man, and Cybernetics 9 (1979): 62-66.